fluids

MDPI

Article

Numerical Study of Heat Transfer Enhancement Using Nano-Encapsulated Phase Change (NPC) Slurries in Wavy Microchannels

Myo Min Zaw, Liang Zhu and Ronghui Ma *

Department of Mechanical Engineering, University of Maryland, Baltimore County, 1000 Hilltop Circle, Baltimore, MD 21250, USA; myo1@umbc.edu (M.M.Z.); zliang@umbc.edu (L.Z.)
* Correspondence: roma@umbc.edu

Abstract: Researchers have attempted to improve heat transfer in mini/microchannel heat sinks by dispersing nano-encapsulated phase change (NPC) materials in base coolants. While NPC slurries have demonstrated improved heat transfer performance, their applications are limited by decreasing enhancement at increased flow rates. To address this challenge, the present study numerically investigates the effects of wavy channels on the performance of NPC slurries. Simulation results reveal that a wavy channel induces Dean vortices that intensify the mixing of the working fluid and enlarge the melting fractions of the NPC material, thus offering a significantly higher heat transfer efficiency than a straight channel. Moreover, heat transfer enhancement by NPC slurries varies with the imposed heat flux and flow rate. Interestingly, the maximum heat transfer enhancement obtained with the wavy channel not only exceeds the straight one, but also occurs at a higher heat flux and faster flow rate. This finding demonstrates the advantage of wavy channels in management of intensive heat fluxes with NPC slurries. The study also investigates wavy channels with varying amplitude and wavelength. Increasing the wave aspect ratio from 0.2 to 0.588 strengthens Dean vortices and consequently increases the Nusselt number, optimal heat flux, and overall thermal performance factor.

Keywords: wavy microchannel heat sink; encapsulated phase change slurries; computational fluid dynamics; electronics cooling; thermal management

check for updates

Citation: Zaw, M.M.; Zhu, L.; Ma, R. Numerical Study of Heat Transfer Enhancement Using Nano-Encapsulated Phase Change (NPC) Slurries in Wavy Microchannels. *Fluids* **2024**, *9*, 236. https://doi.org/10.3390/fluids9100236

Academic Editors: Moran Wang and Goncalo Silva

Received: 16 August 2024
Revised: 18 September 2024
Accepted: 7 October 2024
Published: 9 October 2024

Copyright: © 2024 by the authors. Licensee MDPI, Basel, Switzerland. This article is an open access article distributed under the terms and conditions of the Creative Commons Attribution (CC BY) license (https://creativecommons.org/licenses/by/4.0/).

1. Introduction

With recent advancements in microelectronics [1,2], various cooling techniques such as heat pipes, thermoelectric cooling, jet impingement, microchannel heat sinks, and spray cooling have been developed to address the demand of dissipating the ever-growing heat fluxes with improved efficiency [3–5]. Among these methods, mini/microchannel heatsinks are widely used due to their high heat transfer efficiency, high ratio of heat transfer surface area to fluid volume, compactness, and light weight [6,7].

Since their inception by Tuckerman and Pease in 1981 [8], substantial research interest has been focused on developing efficient working fluids to improve the heat transfer and hydrodynamic performance of mini/microchannel heat sinks. One efficient approach, which is the focus of this study, is to disperse solid phase change materials (PCMs), usually n-octadecane and n-eicosane, in base coolants [9]. With its large heat absorption capacity upon melting (laten heat > 120,000 J/kg), the added phase change material is expected to increase the coolant-specific heat capacity and consequently to enhance the corresponding heat transfer performance. To prevent agglomeration, the phase change material is encapsulated in micro- or nano-sized shells made of flexible materials like polymethyl methacrylate (PMMA) or melamine–formaldehyde resin to accommodate volume changes during the melting and solidification processes [10]. The mixture of a base coolant and an encapsulated phase change material is usually referred to as a micro/nano-encapsulated phase change

slurry (M/NPCS). More information on the thermophysical properties, manufacturing methods, and applications of M/NPCSs can be found in previous reviews [9–11].

Both experimental studies [9,10,12–16] and numerical simulations [17–28] have been conducted to evaluate the heat transfer and hydrodynamic performance of M/NPCS in straight mini/microchannels under a wide range of applied conditions including volumetric concentrations of 5–30 vol.%, Reynolds numbers ranging from 20 to 2000, and heat fluxes up to 500 W/cm^2. A widely used means of quantifying heat transfer enhancement [25–28] is the ratio of the Nusselt number, defined as $Nu_{ratio} = Nu_{NPC}/Nu_{base}$, where Nu_{NPC} and Nu_{base} are the Nusselt numbers obtained with an NPC slurry and a base fluid, respectively.

An Nu_{ratio} greater than one and lowered wall temperatures at the cost of increased pumping power have been reported in previous studies [9,10,12,18–28]. Seyf et al. [20] developed a single-phase model for a tangential impingement of NPC slurries in a microtube. Their results demonstrated a considerable heat transfer enhancement ($Nu_{ratio} > 2$) at the cost of a high pressure drop. The numerical study of Sabbath et al. [22] showed that NPC slurries with volumetric concentrations of less than 20% consumed less pumping power than water to achieve the same heat sink temperature. Kuravi et al. [25] suggested that higher NPC slurry thermal conductivities, narrower channel geometries, and smaller particle sizes would result in better cooling performance. A comprehensive review of the experimental and numerical study of M/NPCS in mini/microchannels can be found in a review paper by Chai et al. [10].

Due to the additional cost of higher pressure loss, the utilization of M/NPCS in microchannel heat sinks must be justified by an impressive heat transfer enhancement over a wide range of flow rates which are necessary to accommodate various levels of heat fluxes generated by devices. Unfortunately, the heat transfer enhancement, indicated by Nu_{ratio}, was found to decrease with increasing flow rates [25]. Additionally, NPC slurries of higher concentrations demonstrate increased Nu_{ratio} only at slower flow rates (Re < 10) [15,16,18,21,22,29], despite their larger latent heat capacity. These observations can be explained by the fact that elevated flow rates reduce the residence time of the NPC slurries in the channel. The result showed a decreased fraction of the melted phase change material, and consequently, a compromised heat transfer enhancement by the M/NPCS.

Besides flow rates and concentrations, heat transfer enhancement by M/NPCS is also dependent on the applied heat fluxes. Dammel and Stephan [15] suggested that the available latent heat should match the supplied heat flux. The results of a two-phase, non-equilibrium model [30,31] explain that heat transfer enhancement and wall temperature reduction mainly occur in the melting region of M/NPCS. Once the slurry temperature at a location exceeds the maximum melting temperature, no enhancement in heat transfer is observed [31]. Alquaity et al. [21] identified an optimal ratio of the heat flux to the mass flow rate that yielded the maximum Nu_{ratio} for a given NPCS concentration in the straight channel, and this optimal ratio increased with the concentration of the NPCS. The range of the identified optimal heat fluxes was 1.5–2.5 W/cm^2.

The persisting difficulties of elevating Nu_{ratio} with high-concentration M/NPCS at increased flow rates is due to poor mixing of the working fluid in the predominantly laminar flow in the microchannel. A fraction of the working fluid outside of the thermal boundary layer remains at temperatures below the melting point. The limited fraction of the melted encapsulated phase change material compromises the amount of the latent heat exploitable to enhance heat transfer efficiency.

Single-phase liquid flow through wavy channels has demonstrated that Dean vortices generated in the sinusoidal path can significantly improve the mixing of the working fluid, resulting in enhanced heat transfer efficiency [32]. A recent experimental study by Reddy et al. [33] investigated the performance of 0.3 vol.% MPCS in straight and wavy minichannels. The results showed that the average Nusselt number in the wavy channel increased by up to 16.7% compared to the base coolant in the straight channel under the same operating conditions, and the corresponding thermal performance factor increased by up to 20% at a Reynolds number of 625. However, understanding of the effect of the

wavy flow path on the melting, convection, and pressure drop of NPC slurries at various flow rates is limited.

Here, we study the heat transfer and flow dynamics of NPC slurries in straight/wavy channels based on a single-phase model, which uses the effective thermal and transport properties to account for the effects of particles in the microchannel flow. For both channel geometries, simulations are performed to determine the Nu_{rattio}, fraction of the melted NPC particles, pressure drop, and optimal heat flux for given flow velocities. Finally, the overall performance of the NPC slurries in different channels is assessed and compared using the thermal performance factor. The influence of the wavy channel wavelength and amplitude on the performance of NPC slurries is also studied.

2. Mathematical Models and Simulation Method

2.1. Problem Setup

The straight and wavy microchannels used in this study, as shown schematically in Figure 1, have an identical width and height of 150 μm and a footprint length of 20 mm. The centerline of the wavy channel is defined as a cosine function, which is $x = A * cos(2\pi z/\lambda)$, where A is the amplitude of the wave and λ is the wavelength. The fluid enters the inlet of the channel at a uniform temperature and velocity. Considering most heat sinks are positioned on top of a chip, one applies a constant heat flux at the bottom of the channel. The top and side walls are insulated, in correspondence to the worst scenario of cooling.

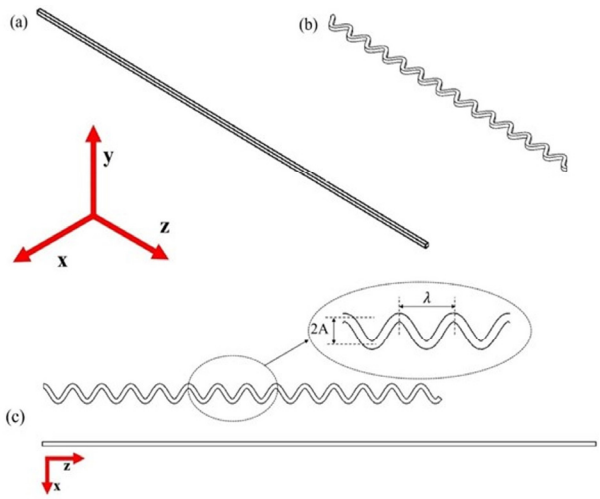

Figure 1. Schematic diagrams of the straight and wavy microchannels used in this study: (**a**) straight channel, (**b**) wavy channel, and (**c**) top view of the straight/wavy channels.

The working fluids used in this study are 10 and 20 vol.% of nano-encapsulated phase change (NPC) particles of 100 nm in diameter dispersed in water. The slurries are simplified as a single-phase fluid where the effects of particles on the fluid flow and heat transfer are aggregated into effective thermophysical and transport properties. For example, the particle–fluid and particle–particle interactions are considered through the effective viscosity and thermal conductivity. Thus, they are not addressed explicitly in the mathematical models.

2.2. Fluid Flow and Heat Transfer Models

The slurries can be assumed incompressible and Newtonian when the particle concentration is less than 30 vol.% [20,25,34]. When evaluating the effective properties of the slurry, we assume that particles are spherical and the particle distribution in the base fluid is uniform. The thermal resistance of the shell is neglected due to its thinness. For nano-sized particles, it is assumed that the temperature in the particle is uniform, and the melting of the core phase change material occurs instantaneously. Gravity is not considered

for the microchannel flow and nano-sized particles. The effect of radiation is negligible for the range of the fluid temperature used in this study. Viscous dissipation is not considered in the energy equation because of the small Renolds numbers in this study (Reynolds number < 100) [35]. The latent heat of the phase change materials is incorporated into the effective specific heat capacity. Finally, only steady-state flow and heat transfer are considered in this study.

With the assumptions described above, the conservation of mass, momentum, and energy for steady-state, single-phase fluid flow and heat transfer in the microchannel are expressed as follows:

$$\frac{\partial u}{\partial x} + \frac{\partial v}{\partial y} + \frac{\partial w}{\partial z} = 0 \tag{1}$$

$$\rho_{eff}\left(u\frac{\partial u}{\partial x} + v\frac{\partial u}{\partial y} + w\frac{\partial u}{\partial z}\right) = -\frac{\partial p}{\partial x} + \frac{\partial}{\partial x}\left(\mu_{eff}\frac{\partial u}{\partial x}\right) + \frac{\partial}{\partial y}\left(\mu_{eff}\frac{\partial u}{\partial y}\right) + \frac{\partial}{\partial z}\left(\mu_{eff}\frac{\partial u}{\partial z}\right) \tag{2}$$

$$\rho_{eff}\left(u\frac{\partial v}{\partial x} + v\frac{\partial v}{\partial y} + w\frac{\partial v}{\partial z}\right) = -\frac{\partial p}{\partial y} + \frac{\partial}{\partial x}\left(\mu_{eff}\frac{\partial v}{\partial x}\right) + \frac{\partial}{\partial y}\left(\mu_{eff}\frac{\partial v}{\partial y}\right) + \frac{\partial}{\partial z}\left(\mu_{eff}\frac{\partial v}{\partial z}\right) \tag{3}$$

$$\rho_{eff}\left(u\frac{\partial w}{\partial x} + v\frac{\partial w}{\partial y} + w\frac{\partial w}{\partial z}\right) = -\frac{\partial p}{\partial z} + \frac{\partial}{\partial x}\left(\mu_{eff}\frac{\partial w}{\partial x}\right) + \frac{\partial}{\partial y}\left(\mu_{eff}\frac{\partial w}{\partial y}\right) + \frac{\partial}{\partial z}\left(\mu_{eff}\frac{\partial w}{\partial z}\right) \tag{4}$$

$$\rho_{eff}\, c_{p,eff}\left(u\frac{\partial T}{\partial x} + v\frac{\partial T}{\partial y} + w\frac{\partial T}{\partial z}\right) = \frac{\partial}{\partial x}\left(k_{eff}\frac{\partial T}{\partial x}\right) + \frac{\partial}{\partial y}\left(k_{eff}\frac{\partial T}{\partial y}\right) + \frac{\partial}{\partial z}\left(k_{eff}\frac{\partial T}{\partial z}\right) \tag{5}$$

where u, v, and w are the velocity components in the x, y, and z directions, respectively; p and T are the pressure and temperature of the fluid, respectively; and ρ_{eff}, μ_{eff}, $c_{p,eff}$ and k_{eff} are the effective density, viscosity, specific heat capacity, and thermal conductivity of the NPC slurry, respectively.

At the channel inlet of $z = 0$, both velocity and temperature are assumed uniform, $u = U_{in}$, $v = w = 0$, and $T = T_{in}$, where U_{in} and T_{in} are the inlet velocity and temperature, respectively. At the outlet $z = L$, $p = 0$, $\frac{\partial T}{\partial z} = 0$. On the channel wall, a no-slip boundary condition is applied, which is $v = u = w = 0$. Thermal insulation is assumed on the top and side walls, $\frac{\partial T}{\partial n} = 0$, where n is the unit vector normal to the wall. A constant wall heat flux, which is $q'' = -k_{eff}\frac{\partial T}{\partial y}$, is applied on the bottom wall, reflecting the heated surface in contact with the heat generating element.

For the flow of NPC slurries in a rectangular channel, the Reynolds number is evaluated using the hydraulic diameter and effective properties, which is

$$Re = \frac{\rho_{eff}\, U_{in}\, D_h}{\mu_{eff}} \tag{6}$$

where D_h is the hydraulic diameter of the channel. The Nusselt number, which measures the strength of the convection heat transfer, is evaluated as follows [20]:

$$\overline{Nu} = \frac{q''\, D_h}{(\overline{T}_w - T_{in})k_{eff}} \tag{7}$$

where $\overline{T}_w$ is the average temperature of the heated wall. $\overline{T}_w$ is calculated based on the area-weighted temperature, expressed as follows:

$$\overline{T}_w = \frac{1}{A_w}\int_{A_w} T_w dA_w \tag{8}$$

where A_w and T_w are the surface area and the temperature of the heated wall, respectively. The pressure drop through the channel determines the pumping power to maintain a

steady flow. It is calculated using the average pressure difference at the inlet and outlet of the channel, which is expressed as follows:

$$\Delta p = \int_{A_{out}} p \, dA_{out} - \int_{A_{in}} p \, dA_{in} \tag{9}$$

where A_{out} and A_{in} are the cross-sectional areas of the outlet and inlet, respectively. The temperature at the outlet of the channel is not uniform. For convenience, the flow rate-weighted mean temperature at the outlet is calculated to represent the average outlet temperature, which is defined as follows:

$$\overline{T}_{out} = \frac{\int_{A_{out}} \rho_{eff} \, u \, c_{p,eff} \, T \, dA_{out}}{\int_{A_{out}} \rho_{eff} \, u \, c_{p,eff} \, dA_{out}} \tag{10}$$

The heat transfer enhancement and power consumption are of special concern when using an NPC slurry as a coolant. The heat transfer enhancement is quantified by the ratio of the Nusselt number obtained with n% NPC in volume to that with pure water (without NPC) in a straight channel under the same operating parameters, which is expressed as follows:

$$Nu_{ratio,n\%} = \frac{\overline{Nu}_{n\%,straight\ or\ wavy}}{\overline{Nu}_{water,\ straight}} \tag{11}$$

Similarly, the increase in pumping power is quantified by the ratio of pressure drop of n% in volume NPC to that with pure water (without NPC) in a straight channel under the same operating parameters, which is

$$\Delta p_{ratio,n\%} = \frac{\Delta p_{n\%,straight\ or\ wavy}}{\Delta p_{water,\ straight}} \tag{12}$$

For an NPC slurry, heat transfer enhancement is achieved at the cost of increased pumping power consumption. Therefore, thermal performance factor (*TPF*) [36–38] has been used to quantify the overall cost-effectiveness of using NPC slurries considering both gain and loss, which is

$$TPF = \frac{Nu_{ratio,n\%}}{(\Delta p_{ratio,n\%})^{1/3}} \tag{13}$$

In addition, a wavy channel induces secondary rotational flow on the plane (x-y) normal to the main streamline, referred to as Dean vortices. The strength of the vortices is directly related to the Dean number, which is defined as follows:

$$De = Re\sqrt{D_h/2R_c} \tag{14}$$

where Re is the channel Reynolds number, and R_c is the radius of the channel curve.

2.3. Effective Properties of NPC Slurries

The NPC slurries used in this study consist of water and paraffin encapsulated in nano-shells with a nominal diameter of 100 nm. When evaluating the effective properties of the slurry, we assume that spherical particles are homogenously distributed in the base fluid and the temperature in the NPC particle is uniform. The effective density and specific heat of a homogeneous slurry are, respectively [34],

$$\rho_{eff} = (1-\varphi)\rho_w + \varphi \, \rho_P, \text{ and} \tag{15}$$

$$c_{p,\ eff} = (1-\varphi)c_{p,w} + \varphi \, c_{p,p} \tag{16}$$

where φ is the mass fraction of the phase change particles. ρ_P and ρ_w are the densities of the phase change material and water, respectively. $c_{p,w}$ and $c_{p,p}$ are the effective specific heat of water and phase change particles, respectively.

For most organic phase change materials, melting or solidification occurs over a range of temperatures, with the lower bound called the solidus temperature T_s, the upper bound the liquidus temperature T_l, and the melting range of the phase change material $T_m = (T_l - T_s)$. Within this melting range, various profiles, such as sinusoidal, step-function, parabolic, etc. have been used to incorporate the latent heat into the effective specific heat $c_{p,p}$ [38]. As the difference in these profiles for the effective specific heat is not critical, as confirmed by Alisetti and Roy [39], a sinusoidal profile is used to express $c_{p,p}$ as a function of temperature, which is

$$For\ T_s < T < T_l, \quad c_{p,p} = c_{p,PCM} + \left\{ \frac{\pi}{2} \left(\frac{h_{sf}}{T_m} - c_{p,PCM} \right) sin\left(\pi \left(\frac{T - T_s}{T_m} \right) \right) \right\} \tag{17}$$

$$For\ T < T_s\ or\ T > T_l,\ c_{p,p} = c_{p,PCM}.$$

where $c_{p,PCM}$ is the actual specific heat of the core phase change materials without phase change.

The effective dynamic viscosity of the slurry is calculated using the following equation [40]:

$$\mu_{eff} = \mu_w \left(1 - \phi - 1.16\,\phi^2\right)^{-2.5} \tag{18}$$

where ϕ is the volumetric fraction of the phase change particles and μ_w is the dynamic viscosity of water.

The effective medium theory developed by Maxwell for dispersed particles [41] has been widely used to evaluate the effective thermal conductivity of nanoparticle suspensions. A benchmark experimental study of effective thermal conductivity of nanofluids [42] reported a good agreement between the Maxwell model and the experimental data. Therefore, the Maxwell model is used in this study for calculating the effective thermal conductivity of the slurry, which is

$$k_{eff} = k_w \frac{2 + \frac{k_{PCM}}{k_w} + 2\,\phi\left(\frac{k_{PCM}}{k_w} - 1\right)}{2 + \frac{k_{PCM}}{k_w} - \phi\left(\frac{k_{PCM}}{k_w} - 1\right)} \tag{19}$$

where k_{PCM} and k_W are the thermal conductivities of the phase change material and water, respectively.

2.4. Fluid Properties, Simulation Parameters, and Numerical Issues

The thermophysical properties of the base coolant, which is water, and PCM particles are listed in Table 1. For the NPC slurries, the range of melting temperatures can be adjusted by additives. This study uses a very narrow melting range of 1 K to isolate the effect of the melting range on heat transfer enhancements by channel shape.

Table 1. Water and paraffin properties for the single-phase model [20,43,44].

Water	Density, ρ_w (kg/m^3)	998.2
	Viscosity, μ_w (Pa s)	0.001003
	Specific heat capacity, $c_{p,w}$ (J/K)	4182
	Thermal conductivity, k_w (W/mK)	0.6

Table 1. *Cont.*

Paraffin (PCM)	Density, ρ_{PCM} (kg/m^3)	850
	Specific heat capacity, $c_{p,PCM}$ (J/(kgK))	1800
	Thermal conductivity, k_{pcm} (W/(mK))	0.34
	Latent heat of fusion, h_{sf} (J/kg)	220,300
	Solidus temperature, T_s (K)	300
	Liquidus temperature, T_l (K)	301

The continuity, momentum, and energy equations (Equations (1)–(5)) were solved with the finite volume method using the commercial package ANSYS-Fluent® (2019, R2). The three-dimensional geometries of the straight and wavy channels were created in SOLIDWORKS® (2019) and then meshed by ANSYS-Mesh (2019, R2) using cube-shaped elements. The second-order upwind scheme was used to discretize the convection and diffusion terms. The built-in SIMPLE scheme of the software was chosen for pressure–velocity coupling. The convergence criteria for the residuals of momentum and energy were at 10^{-6} and 10^{-12}, respectively.

Mesh dependence studies were performed in the straight and wavy channels using an inlet velocity of U_{in} = 0.46 m/s and a bottom surface heat flux of 16 × 10^4 W/m^2. The simulation results showed that increasing the number of elements from 202,500 to 500,000 resulted in a difference of less than 0.04% in the average wall temperature and a difference of less than 2% in the pressure drop in both the straight and wavy channels. Thus, 202,500 elements were used for the present study.

2.5. Model Validation

To validate the numerical model, simulations were first conducted to determine the Nusselt numbers of water in the straight and wavy channels in which the geometries and flow conditions were prescribed by Sui et al. [45]. The straight and wavy channels were 205 µm in width, 404 µm in height, and 25 mm in footprint length. The wavy channel had a sinusoidal profile with a wavelength λ of 2.5 mm and an amplitude A of 138 µm. The inlet temperature was 300 K, and at the bottom wall of the channel, a uniform heat flux of 50 × 10^4 W/m^2 was applied. As presented in Figure 2a, the predicted overall Nusselt numbers in the present study agree well with the experimental results reported by Sui et al. [45], indicated by the maximum percentage difference of 6.25%.

The simulation of heat transfer with aqueous slurries of 2 vol.% phase change material (paraffin) in the straight channels was validated with the experimental study conducted in millimeter-sized channels by Wang et al. [46]. The square channel used in this study was 0.35 mm in width and height and 440 mm in length. A uniform heat flux of 6083 W/m^2 was applied at the bottom of the channel. As shown in Figure 2b, the maximum percentage difference between the present study and the experimental result was 6.85% for Reynolds numbers over the range of 300–1200, indicating a reasonably good agreement.

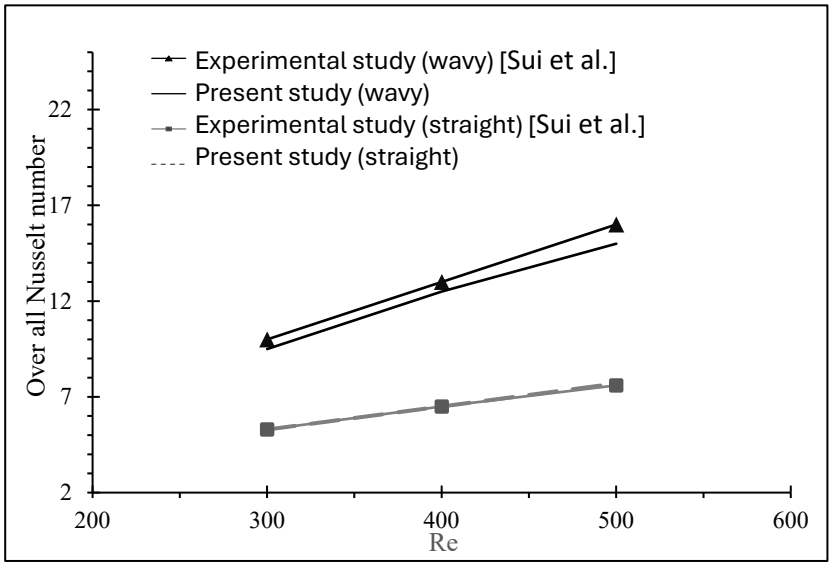

(**a**)

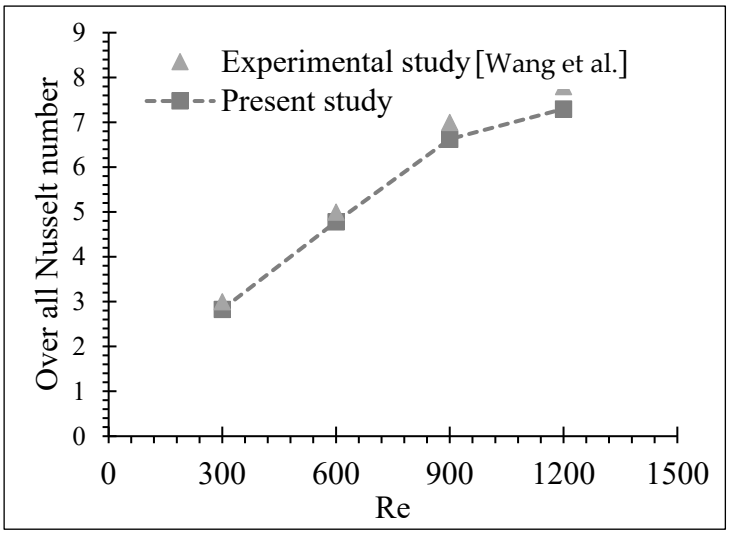

(**b**)

Figure 2. (**a**) Comparison of overall Nusselt numbers from the present study with the experimental results of Sui et al. [45]. (**b**). Comparison of overall Nusselt numbers from the present study with the experimental results of Wang et al. [46].

3. Results and Discussion

The fluid flow dynamics and heat transfer of NPC slurries in straight and wavy channels were studied using the numerical model described in the previous section. Simulations were first conducted to elucidate the effects of the wavy channel flow on the flow pattern and the resulting changes in the temperature distribution, the fraction of the melted NPCs, and the Nu_{ratio} at various applied heat fluxes and inlet velocities (Table 2) for 10 and 20 vol.% NPC slurries. Then, the optimal applied heat flux that gave the maximum heat transfer enhancement, as indicated by Nu_{ratio}, was identified for a given inlet velocity, followed by assessment of cost-effectiveness through determination of the pressure drop and thermal performance factors (*TPFs*). Finally, the effect of wavy channel configurations (such as wavelength and amplitude) on heat transfer enhancement and pressure drop were evaluated.

Table 2. Applied heat fluxes and inlet velocities.

Variable	Value			
Heat flux (W/m^2) for 10 vol.% NPCS	2×10^4	4×10^4	6×10^4	8×10^4
Inlet velocity (m/s)	0.11	0.21	0.32	0.42
Heat flux (W/m^2) for 20 vol.% NPCS	4×10^4	8×10^4	12×10^4	16×10^4
Inlet velocity (m/s)	0.12	0.23	0.35	0.46
Inlet temperature (K)	300			

3.1. Effect of the Wavy Channel on the Heat Transfer and Fluid Flow of NPC Slurries

For 10 vol.% NPC slurry, the applied heat fluxes listed in Table 2 are 2×10^4, 4×10^4, 6×10^4, and 8×10^4 W/m^2. Doubled heat fluxes, which are 4×10^4, 8×10^4, 12×10^4, and 16×10^4 W/m^2, are used as the NPCS concentration increases to 20 vol.%. When selecting the inlet velocity for each applied heat flux, we consider an ideal situation in which the inlet and outlet temperatures of the slurry coincide with the solidus and liquidus temperature, which are T_s and T_l, respectively. Furthermore, the slurry is perfectly mixed at all locations in the channel so that the phase change particles become completely melted at the outlet. Under these hypothetical conditions, the effective specific heat capacity of the working fluid reaches its maximum value ($c_{p,max}$) and, consequently, produces the highest possible enhancement of heat transfer. The maximum $c_{p,max}$ can be expressed as [34]

$$c_{p,max} = \left[(1-\varphi)c_{p,w} + \frac{\varphi\, h_{sf}}{T_l - T_s}\right] \tag{20}$$

Based on the principle of energy conservation, the inlet velocity U_{in} that allows the slurry to reach the target outlet temperature, T_l, for an applied heat flux q'' is

$$U_{in} = \frac{q''\, A_W}{\rho_{eff}\; A_c c_{p,max}(T_l - T_s)} \tag{21}$$

where A_c is the cross-sectional area of the channel. Therefore, for both slurry concentrations (10 and 20 vol.%), the inlet velocity increases proportionally with the applied heat flux over the range of 0.1 to 0.5 m/s, as given in Table 2. The corresponding range of the Reynolds number is 10 to 80, which suggests a laminar flow in the microchannels.

The temperature fields on the *x*-*y* plane at the outlet of the straight channel with 10 and 20 vol.% NPCS are displayed in Figures 3a and 3b, respectively. As displayed in Figure 1, the *x*-*y* plane coincides with the cross-section of the channel. For all the cases in the straight channel, the temperature fields are symmetric with respect to the vertical centerline of the cross-section. For each applied heat flux, the highest temperature, which is above the liquidus temperature of 301 K, is found at the bottom; a nearly flat isothermal line indicates an insignificant temperature variation across the bottom surface. The liquid temperature near the top surface, which is insulated, remains close to the inlet condition of 300 K. Additionally, the volume of the liquid having the temperature close to the inlet temperature of 300 K (deep blue color) is observed to increase with the increased inlet velocity, even though the applied heat flux increases proportionally with the inlet velocity. As shown in Figure 3d, the highest temperature at the bottom surface is 322.2 K, which is below the boiling temperature of water.

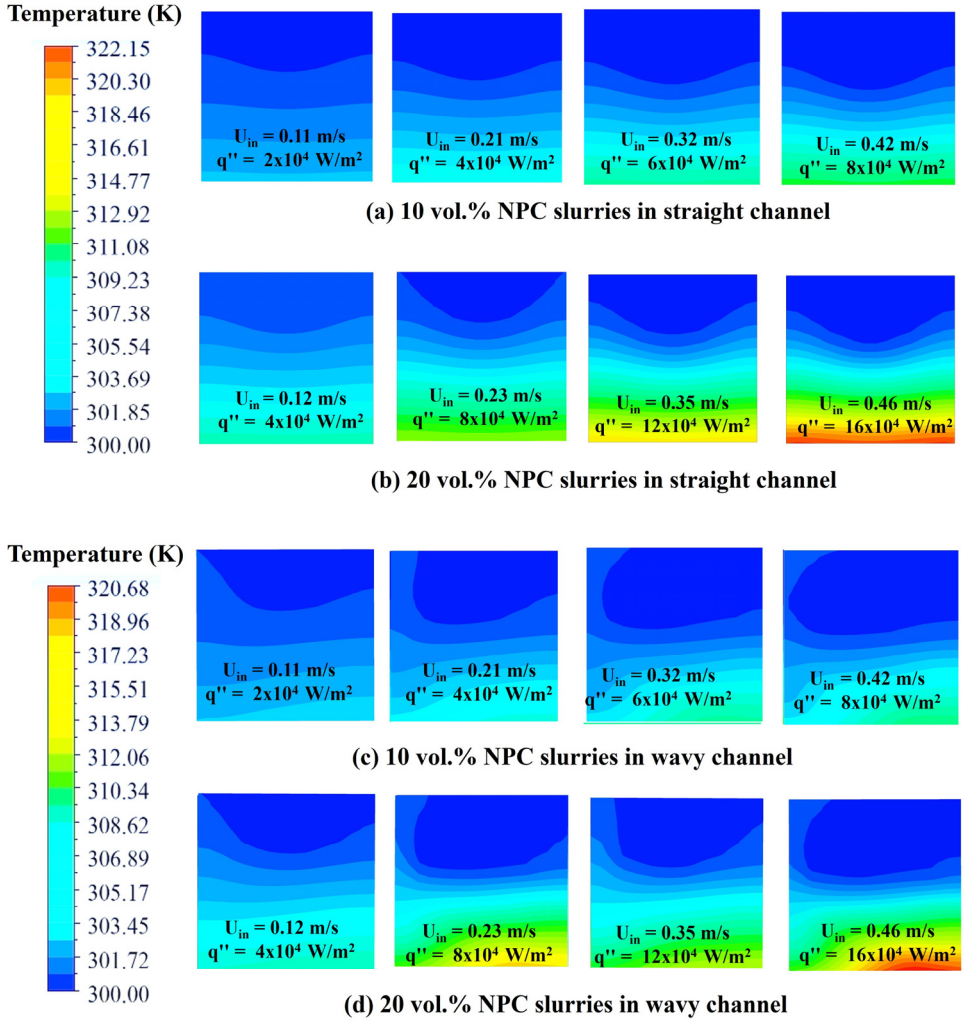

Figure 3. Temperature distributions on the *x*-*y* plane at the outlet of the straight and wavy channels: (**a**) straight channel with 10 vol.% NPC slurries; (**b**) straight channel with 20 vol.% NPC slurries; (**c**) wavy channel with 10 vol.% NPC slurries; (**d**) wavy channel with 20 vol%. NPC slurries.

Considering the laminar nature of the channel flow, the observed features, such as symmetry and little temperature variation across the bottom surface, were expected due to the poor mixing in the channel. The large volume of liquid at the inlet condition near the top wall indicated that the thermal boundary layer was not yet fully developed, and the thickness of the thermal boundary decreased with the inlet velocity.

The fractions of the melted NPC on the same *x*-*y* plane at the outlet of the straight channel with 10 and 20 vol.% NPCSs are plotted in Figures 4a and 4b, respectively. As melting is temperature-dependent, the fraction of the melted NPC particles varied on the cross-section, following a pattern similar to the corresponding temperature distribution, such as a symmetrical distribution with respect to the vertical centerline. In addition, for all the cases in the straight channel, the slurry near the bottom was completely melted because the local temperature was above the liquidus temperature (301 K). Near the top surface, the NPC was observed to be either partially melted or in the solid phase because the local temperature was close to or at the inlet condition of the solidus temperature. Moreover, the fraction of the NPC remaining in the solid phase increased with the increasing inlet velocity, which was consistent with the increasing volume of the liquid at temperatures near 300 K at high inlet velocities, as shown in Figure 3a,b.

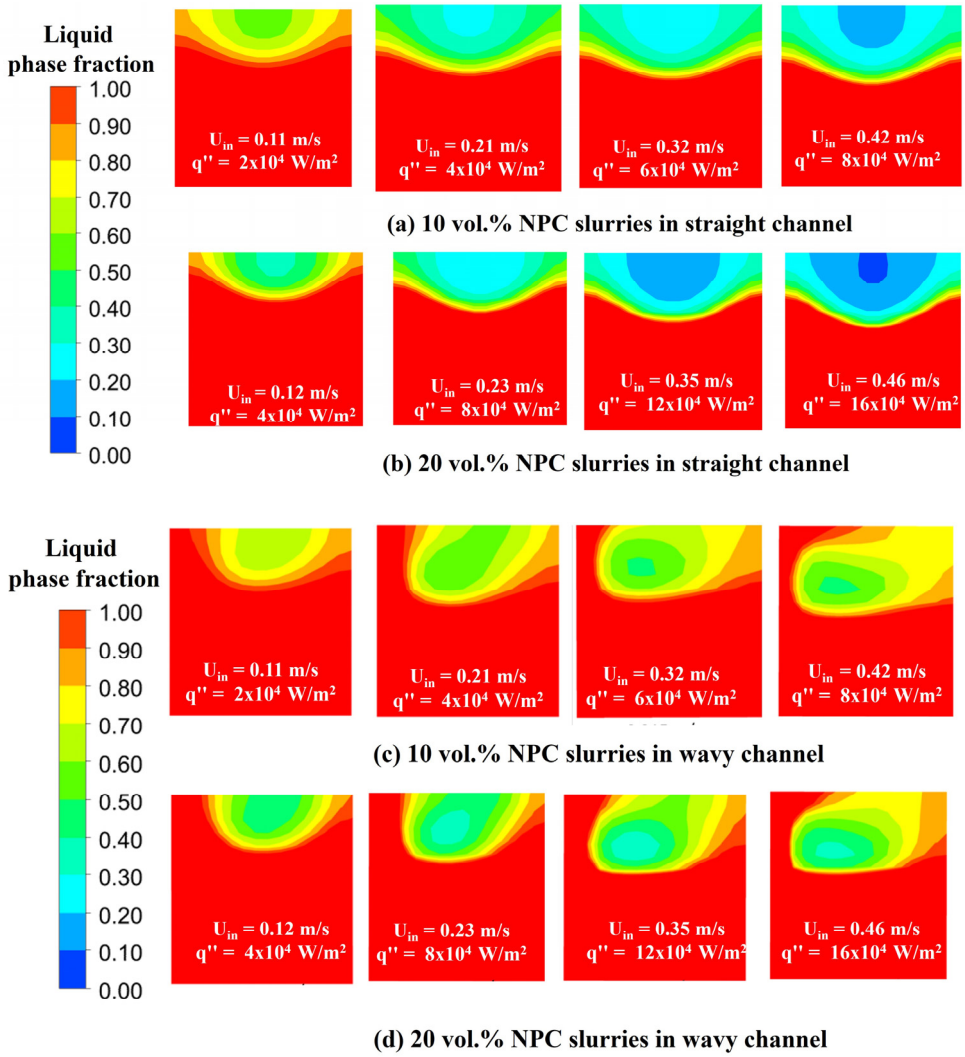

Figure 4. The melted fractions of NPC particles on the *x*-*y* plane at the outlet of straight and wavy channels: (**a**) straight channel with 10 vol.% NPC slurries; (**b**) straight channel with 20 vol.% NPC slurries; (**c**) wavy channel with 10 vol.% NPC slurries; (**d**) wavy channel with 20 vol%. NPC slurries.

Interestingly, the distributions of both the temperature and the fraction of the melted NPC changed in the wavy channels. Figure 3c,d display the temperature distributions in the wavy channel for 10 and 20 vol.% NPC slurries, respectively, and Figure 4c,d show the distributions of the fraction of the melted NPC slurry. Notably, the symmetric feature exhibited in the straight channels (Figures 3a,b and 4a,b) was disrupted by the wavy flow path. While the temperature at the bottom was above the liquidus temperature of 301 K, as in the straight channels, the temperature across the bottom surface varied, with the highest temperature being near the outside wall in the radial direction of the channel curve.

The effects of the differing temperature distributions induced by the wavy channel were obvious. For the 10 vol.% NPC slurry passing the straight channels at four inlet velocities of 0.11, 0.21, 0.32, and 0.42 m/s, the respective fractions of the melted NPC given in Table 3 are 0.88, 0.85, 0.82, and 0.76. The wavy flow path increased the fractions of the melted NPC, which are 0.94, 0.92, 0.87, and 0.84, respectively for the same inlet velocities. Therefore, the respective increases in the melted fraction of the NPC in the wavy flow channels at the four inlet velocities are 6.38%, 8.24%, 6.09%, and 7.89%.

Table 3. The simulated NPC melted fraction and the maximum vorticity (wavy channels only).

10 vol.% NPC slurries					
Inlet velocity (m/s)		0.11	0.21	0.32	0.42
Heat flux (W/m^2)		2×10^4	4×10^4	6×10^4	8×10^4
Fraction of melted NPC	(Straight)	0.88	0.85	0.82	0.76
	(Wavy)	0.94	0.92	0.87	0.84
Maximum vorticity (1/s)	(Wavy)	950	4725	6694	11,813
20 vol.% NPC slurries					
Inlet velocity (m/s)		0.12	0.23	0.35	0.46
Heat flux (W/m^2)		4×10^4	8×10^4	12×10^4	16×10^4
Fraction of melted NPC	(Straight)	0.92	0.88	0.86	0.80
	(Wavy)	0.96	0.92	0.90	0.89
Maximum vorticity (1/s)	(Wavy)	945	4659	6633	11,722

Like the 10 vol.% slurries, more NPC from the 20 vol.% NPC slurries was melted in the wavy channel, evidenced by the larger fractions of the melted NPC (0.96, 0.92, 0.90, and 0.89, respectively, for the inlet velocities of 0.12, 0.23, 0.35 and 0.46 m/s). Compared with the respective fractions of the melted NPC in the straight channel, which were 0.92, 0.88, 0.86, and 0.80 for the same set of inlet velocities, the respective increase in the wavy channels was 4.35%, 4.55%, 4.65%, and 11.25%. One should note that for the 20 vol.% NPC slurries, the applied heat fluxes doubled, and the inlet velocities increased accordingly (Equation (21)), as shown in Table 3.

The increased fractions of the melted NPC slurry had an interesting impact on the overall Nusselt number ratios, which assesses heat transfer enhancement by comparing the Nusselt numbers of the NPC slurry with those of the base coolant. Plotted in Figure 5 is Nu_{ratio} at various inlet velocities for the 10 and 20 vol.% slurries. In the straight channels, the Nu_{ratio} decreases steadily with the inlet velocities, thus agreeing with results reported in a previous study [25]. The main reason for this is that the fraction of the melted NPC declined with the inlet velocities, as shown in Figure 4a,b, due to the shortened amount of time that it resided in the channel.

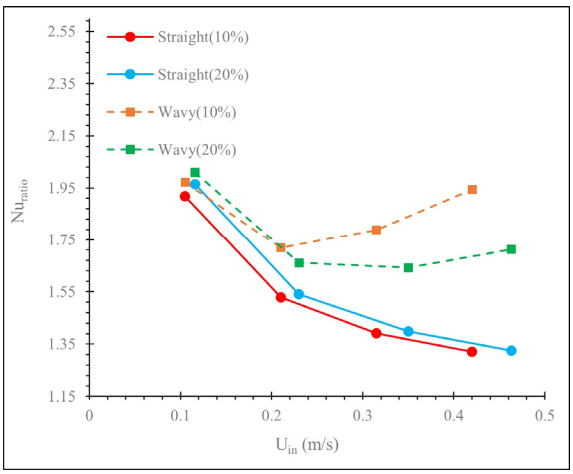

Figure 5. Variations in Nu_{ratio} with the inlet velocity in the straight and wavy channels for different NPC concentrations.

Interestingly, the Nu_{ratio} of the wavy channel displays a trend differing from that of the straight channel. This observation can be attributed to the secondary rotating flow on the plane normal to the mainstream of the channel flow, as displayed in Figure 6a,b for 10 vol.% NPC slurries. These vortices, referred to as Dean vortices, are generated as the fluid passes a curved channel in which the fluid elements near the channel centerline move faster than those near the wall. Driven by inertia, these high-momentum fluid elements tend to continue along the tangential direction of the curved path. The outward motion of the fluid element creates a pressure gradient in the radial direction (normal to the curve). This pressure gradient forces the sluggish fluid elements near the channel wall to flow inwards along the circumference of the channel, forming two counter-rotating streams, shown in Figure 6b. The patterns of the vortices for the 20 vol.% NPC slurry are similar to those in Figure 6 and are not presented here.

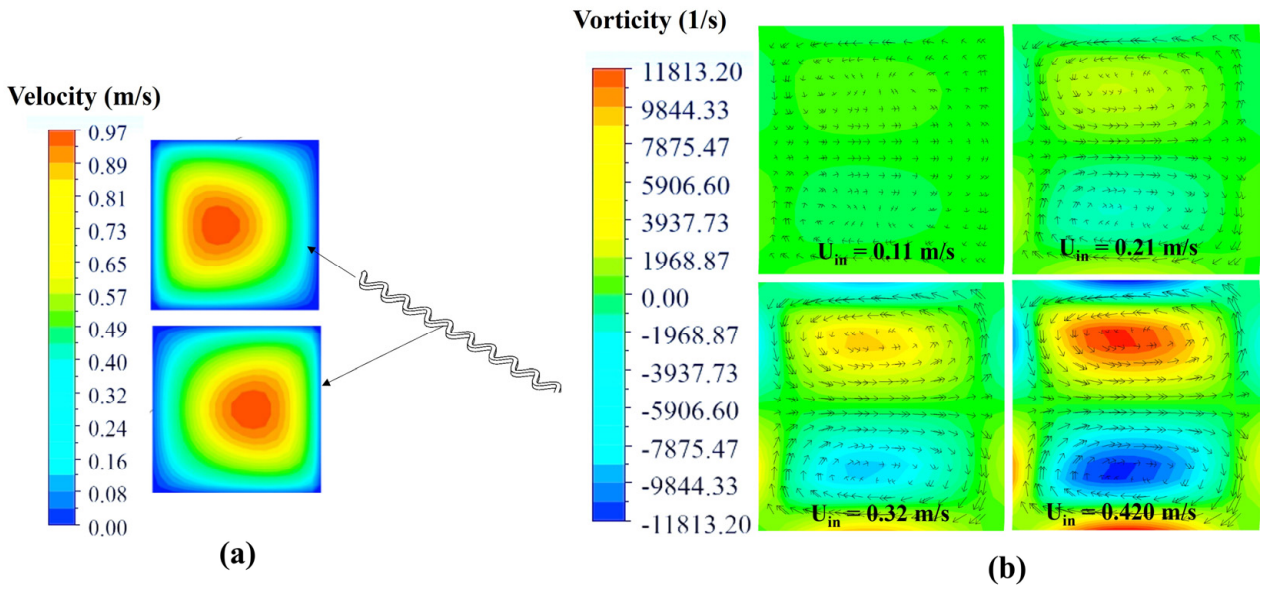

Figure 6. (**a**) Distributions of velocity over the channel cross-section at the peak and trough of the wavy channel for U_{in} = 0.42 m/s with 10 vol.% NPC; (**b**) the vorticy at the peak of the wavy channel at various inlet velocities.

The impact of Dean vortices can be clearly seen in the distorted profiles of temperature (Figure 3c,d) and the fraction of the melted NPC (Figure 4c,d). Dean vortices initiate the mixing of the NPC slurry on the plane normal to the channel flow. Additionally, the rotating direction of the vortices alternates from one peak to the next in the wavy channel, as presented in Figure 6a, which further intensifies the mixing outcome. Improved mixing of the NPC slurry enlarges the fractions of the melted NPC and results in a higher Nu_{ratio} than the straight channel, as shown in Table 3 and Figure 5.

The strength of the Dean vortices is characterized by the De number given in Equation (14). It increases with the Re of the mainstream flow, the squre root of the hydraulic diameter of the channel (D_h), and the squreroot of the curvature ($1/R_c$). For given channel dimensions and coolant properties, the main stream velocity is a critial factor, evidenced by the emergence of the vortices as the mainstream velocity increases from 0.11 to 0.42 m/s in Figure 6b. In Table 3, the maximum vorticity for a 10 vol.% slurry is observed to increase from 950 1/s at an inlet velocity of 0.11 m/s to 11,813 1/s at an inlet velocity of 0.42 m/s.

The velocity-dependent strength of Dean vortices explains the reason why heat transfer enhancement by the wavy channel is only pronounced at elevated velocities. For example, the Nu_{ratio} of the wavy channel decreases first, reaching an extremum point at inlet velocities of 0.21 m/s and 0.35 m/s for the 10 and 20 vol.% NPC slurries, respectively, before it rises. As shown in Figure 6b, the Dean vortices are barely visible for inlet velocities below 2.1 m/s for the 10 vol.% NPC slurry. Due to the limited mixing at low inlet velocities, heat transfer

is still dominated by the residence time of the NPC particles in the channel, as indicated by the declining trend in the Nu_{ratio}, similar to that in the straight channels. However, beyond an inlet velocity of 2.1 m/s, the growing strength of the Dean vortices prevails over the shortened residence time, giving rise to an increasing Nu_{ratio}. It is ancipated that the Nu_{ratio} will continue to increase at the inlet velocities in excess of 0.5 m/s for NPCSs of both concentrations.

Additionally, Figure 5 reveals that the Nu_{ratio} values obtained with 10 vol.% slurries are higher than that with the 20 vol.% slurry in the wavy channel. This can be explained by the influence of the slurry concentration on the vorticitiy through the effective viscosity, as shown in Equation (18). When the inlet velocities are similar, a slightly higher maximum vorticity is observed for the 10 vol.% slurry than the 20 vol.% in Table 3. For example, the maximum vorticity for the 10 vol.% slurry is 6694 1/s at 0.32 m/s, which is 0.9% higher than the vorticity of 6633 1/s at 0.35 m/s for the 20 vol.% slurry.

These results reveal that Dean vortices created in the wavy flow path can give rise to substantial mixing of the working fluid on the plane normal to the mainstream flow, leading to a beneficial outcome, such as increased fractions of the melted NPC and enhanced heat transfer efficiency. Furthermore, the impact of the wavy channels on heat transfer enhancement is more pronounced at high velocities and lower NPC concentrations.

3.2. Optimal Heat Flux for an Inlet Velocity in the Straight and Wavy Channels

At a given inlet velocity, the heat transfer enhancement (Nu_{ratio}) achieved by the NPC slurry is also dependent on the applied heat flux. For 10 vol.% slurries, simulations were carried out for both straight and wavy channels to determine the Nu_{ratio} at four inlet velocities of 0.11, 0.21, 0.32, and 0.42 m/s, with the applied heat fluxes ranging from 2×10^3 to 5×10^4 W/m^2. The simulation was then repeated for 20 vol.% slurries for inlet velocities of 0.12, 0.23, 0.35, and 0.46 m/s, with the applied heat fluxes varying within the range of 5×10^3 to 10^5 W/m^2.

The results of the 10 and 20 vol.% slurries in the straight channel are presented in Figures 7a and 7b, respectively. For each inlet velocity, the Nu_{ratio} first increased with the applied heat flux. However, after reaching a peak value, it declined steadily. The heat flux that produced the peak Nu_{ratio} is referred to as the optimal heat flux. For both NPC concentrations, the peak Nu_{ratio} value declined as the inlet velocity increased.

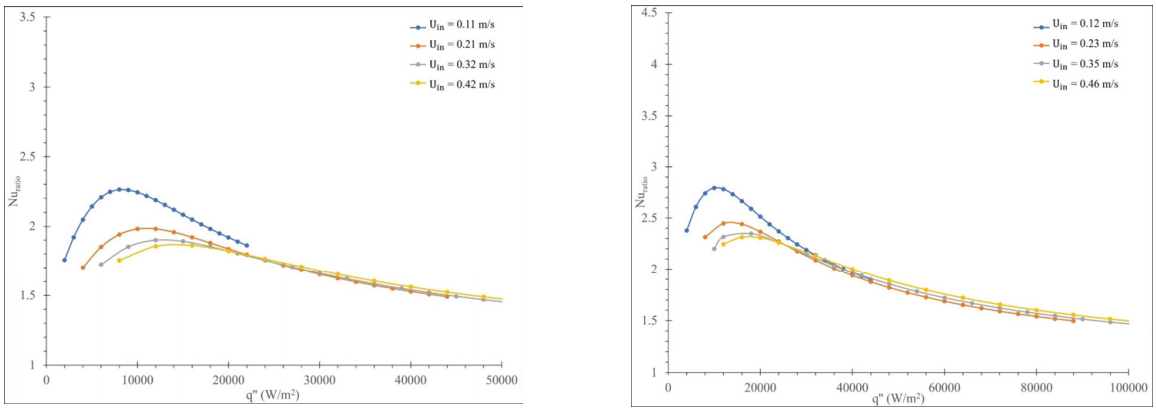

(**a**) (**b**)

Figure 7. Nu_{ratio} vs. heat flux at various velocities in straight channel with (**a**) 10 vol.% and (**b**) 20 vol.% NPC slurries.

For 10 vol.% NPC slurries, the best heat transfer enhancement among the four inlet velocities was Nu_{ratio} = 2.26, obtained at the lowest inlet velocity of 0.11 m/s and the optimal heat flux of 8000 W/m^2 (over the range of 2×10^3 to 5×10^4 W/m^2). The same trend was observed in the slurries of a higher concentration (20 vol.%), as shown in Figure 7b.

The best heat transfer enhancement, Nu_{ratio} = 2.79, occurred at the lowest inlet velocity of 0.12 m/s, and the corresponding optimal heat flux was 1.4 × 10^4 W/m^2. To summarize, the best heat transfer enhancement in the straight channels with 10 and 20 vol.% NPC slurries was found at the wall heat fluxes < 1.5 × 10^4 W/m^2 and the inlet velocities < 0.2 m/s.

The NPCSs' flow in the wavy channel gave rise to differing trends in Nu_{ratio} versus applied heat fluxes, which are presented in Figure 8a,b for the 10 and 20 vol.% NPC slurries, respectively. For the 10 vol.% NPC slurry, the best Nu_{ratio} of 3.32 was obtained at the highest inlet velocity of 0.42 m/s and the applied heat flux of 2 × 10^4 W/m^2. The wavy channel demonstrated a 46.90% increase in heat transfer enhancement and a 50% increase in the optimal heat flux when compared with the straight channel (Nu_{ratio} = 2.26 and q'' = 8000 W/m^2). For the 20 vol.% NPC slurry, the best Nu_{ratio} of 4.25 was again obtained at the highest inlet velocity of 0.45 m/s and an optimal heat flux of 3.2 × 10^4 W/m^2. The wavy channel demonstrated a 52.33% increase in heat transfer enhancement and a 29% increase in the optimal heat flux when compared with the straight channel (Nu_{ratio} = 2.79, q'' = 1.4 × 10^4 W/m^2). This comparison demonstrates the ability of the wavy channel to offer better heat transfer enhancement at higher flow rates and more intensive applied heat fluxes.

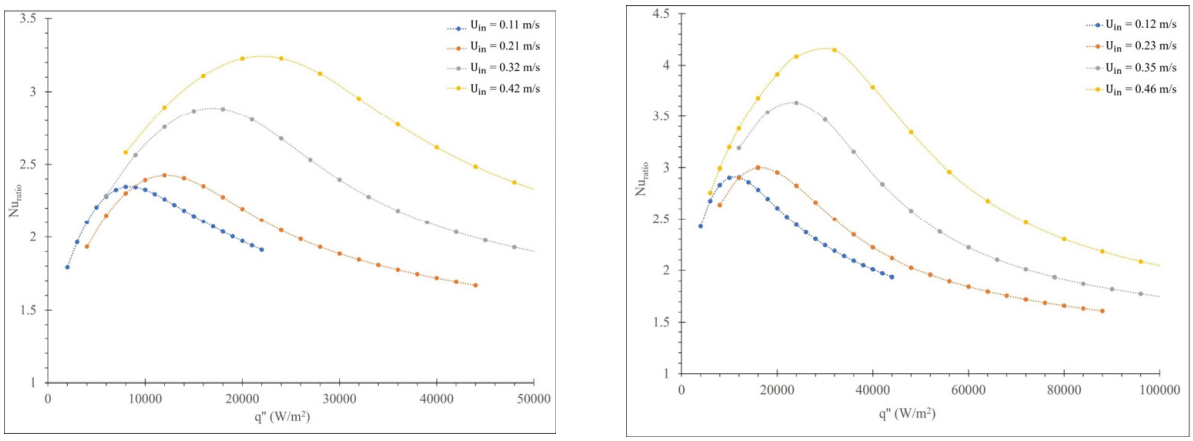

(**a**) (**b**)

Figure 8. Nu_{ratio} vs. heat flux at various inlet velocities in the wavy channel (**a**) using 10 vol.% NPC slurries; (**b**) using 20 vol.% NPC slurries.

The existence of an optimal heat flux that maximizes the heat transfer enhancement at a given velocity can be related to the Stefan number for phase change and heat transfer of the NPC slurry in microchannels. The Stefan number (Ste) is defined as $c_p(\Delta T)/H$, where ΔT is the increase in the temperature of the slurry between the inlet and outlet, c_p is the specific heat capacity of the working fluid without phase change, and H is the actual latent heat proportional to the fraction of melted NPC slurry. A small Ste number means a large fraction of the NPC particles melts over a narrow ΔT, which is indicative of a great enhancement in heat transfer. The correlation between a high Nu_{ratio} and a small Ste has been reported in a number of published studies [13–16,20,21].

For an NPC flow in a straight channel at a constant inlet velocity, the applied heat flux has an impact on both ΔT and the fraction of the melted NPC particles. As the applied heat flux increases from a low value, the Ste number first decreases because the latent heat absorbed by the NPC particles suppresses ΔT. However, as the thermal boundary layer is not fully developed in the channel, as shown in Figure 3a, the amount of latent reaches its maximum when all the particles within the thermal boundary layer are melted. However, ΔT continues to increase with the applied heat flux, as does the Stefan number. Therefore, a minimum Ste exists, giving rise to a maximum Nu_{ratio}.

Additionally, the maximum Nu_{ratio} varies with the inlet velocity. At low velocities, the NPC particles are heated over a longer period of time in the channel, leading to a larger

fraction of the melted NPC particles, as shown in Figure 4a. Therefore, the best Nu_{ratio} occurs at the lowest velocity for both concentrations of the NPC slurries. On the other hand, ΔT increases quickly as the heat flux is more intensive. This is the reason that the best Nu_{ratio} is found not only at low velocities but also at low heat fluxes in the straight channel for both NPC concentrations.

In contrast, the best Nu_{ratio} value of the wavy channels is observed at the highest inlet velocity in the simulation, illustrating that at high inlet velocities, the effects of Dean vortices on the fraction of the melted particles prevail over the shortened residence time. As a result, the Stefan number decreases as the inlet velocity increases. Further, the larger fraction of the melted particles and the higher flow rate can accommodate higher heat fluxes without a substantial increase in ΔT. Therefore, both the maximum Nu_{ratio} and the optimal heat flux increase with the inlet velocity, as shown in Figure 8.

3.3. Pressure Drop and Thermal Performance Factor

One concern with utilization of NPC slurries and wavy channels in microchannel heat sinks is the increased pressure drop that necessitates more power consumption and/or the larger capacity of the pump. In addition to the higher viscosities of the particulate fluids than the single-phase base coolant, the wavy flow path gives rise to an extra pressure drop due to Dean vortices that rotate in the direction normal to the mainstream. This negative outcome is usually characterized by the pressure drop ratio defined in Equation (12), which is the ratio of the pressure drop with NPC slurries in a straight/wavy channel to that of the pure base coolant (water) in a straight channel, given the identical foot length and cross-sectional dimensions of the channels.

The pressure drop ratios for the straight and wavy channels are compared in Figure 9a. In the straight channel, the respective flow pressure ratio is approximately 1.3 and 2.0 for the 10 vol.% and 20 vol.% NPC slurries at the inlet velocities of 0.11 and 0.12 m/s. Additionally, no substantial change in the pressure drop ratio is observed when increasing the inlet velocity. Based on the fluid mechanics of laminar flow through straight channels [47], the pressure drop is $\Delta p = ½\, \rho\, V^2 f L/D_h$, where L is the length of the channel and f is the friction factor. As $f = 64/Re$ for laminar flow, the pressure ratio becomes dependent on the ratio of viscosity only. Therefore, the pressure drop ratio remains nearly constant as the inlet velocity increases.

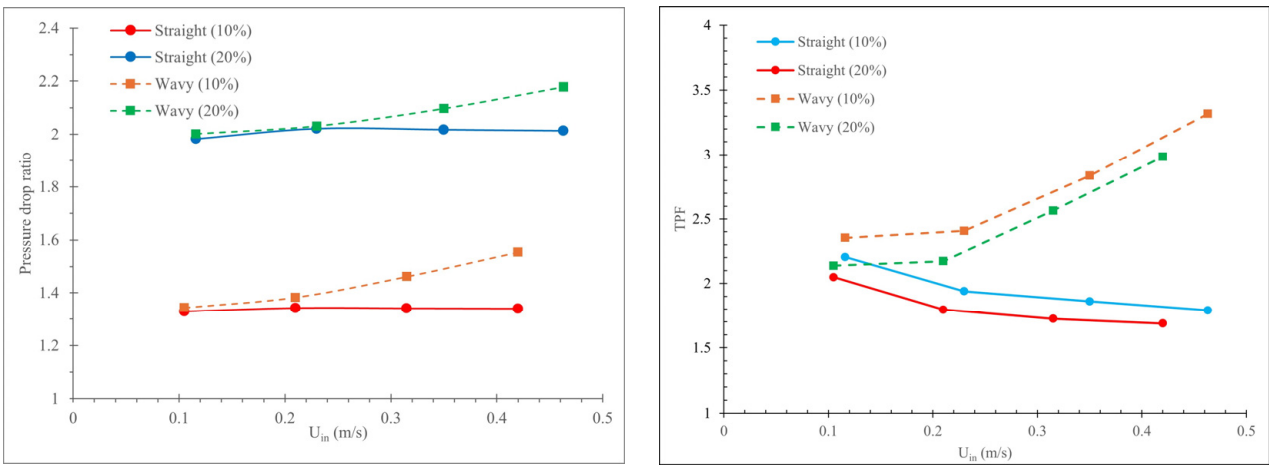

(**a**) (**b**)

Figure 9. (**a**) Pressure drop ratio at various velocities and NPC concentrations; (**b**) thermal performance factor at various velocities and NPC concentrations for straight and wavy channels. Optimal heat fluxes are used in *TPF* calculation.

In contrast, the pressure drop ratios of the wavy channel exhibit an upward trend due to Dean vortices that intensify with the mainstream velocity. The increase is not substantial until the inlet velocity exceeds 0.2 m/s for both slurry concentrations. This corroborates the dependence of the strength of Dean vortices on the mainstream velocities. The pressure drop ratio increases from 1.3 to 1.5 (15.4% increase) when the inlet velocity increases from 0.11 to 0.42 m/s for 10 vol.% NPC slurries, and from 2 to 2.17 (8.5% increase) when the inlet velocity increases from 0.12 to 0.45 m/s for 20 vol.% NPC slurries.

In microchannels, the increase in heat transfer enhancement is always associated with a greater pressure drop. It is therefore necessary to assess the cost-effectiveness of NPC slurries and wavy channels. The thermal performance factors (*TPFs*), defined in Equation (13) as the ratio of Nu_{ratio} to the cubic root of the corresponding pressure drop, have been used for this purpose [36]. The variations in *TPFs* with inlet velocities ranging from 0.1 to 0.5 m/s for 10 and 20 vol.% slurries are plotted in Figure 9b. It is worth mentioning that the *TPF* value for each inlet velocity is calculated using the maximum Nu_{ratio} values given in Figures 7 and 8, which correspond to the optimal heat flux.

The overall benefit of NPC slurries in straight/wavy channels is demonstrated by the *TPF* > 1 for all the cases. However, the *TPF* for the straight channel decreases with increasing velocity for the slurries of both concentrations. A 17.1% decrease (from 2.1 to 1.7) is observed for 10 vol.% slurries when the inlet velocity increases from 0.11 to 0.42 m/s. A similar decrease of 18.2% (from 2.2 to 1.8) is found for 20 vol.% NPC slurries when the inlet velocity increases from 0.12 to 0.45 m/s. The decreasing trends discourage the utilization of NPC slurries in situations wherein high coolant flow rates are necessary to keep the bottom temperature below a given threshold.

In contrast, the *TPF* in the wavy channel exhibits increasing trends with the inlet velocities for both slurry concentrations. The *TPF* increases from 2.14 to 3.0 (40.2% increase) with the increasing inlet velocity from 0.12 to 0.45 m/s for 10 vol.% NPC slurries and from 2.36 to 3.31 (40.3%) with the increasing inlet velocity from 0.11 to 0.42 m/s for 20 vol.% NPC slurries. The increasing trend confirms that the combination of NPC slurries and wavy channels is favorable for heat transfer enhancement.

3.4. Effect of Wavelengths and Amplitude on Heat Transfer Performance

The De number (Equation (14)) is proportional to the square root of the curvature, $1/R_c$. Varying the wavelength or the amplitude, or both of a wavy channel can alter the maximum curvature, which significantly impacts the intensities of Dean vortices [47–52] and the heat transfer and hydraulic performance. The wave aspect ratio γ, defined as the ratio of the amplitude (A) to the wavelength (λ) has been also used [52–54] to illustrate the combined impact of these two parameters. For single-phase coolants, the effects of various combinations of wavelength and amplitude on the *Nusselt* number and the pressure drop have been tested under either a fixed Reynolds number [52–54] or pumping power [48,50]. It is important that we understand how these parameters affect the hydraulic and heat transfer performance of NPC slurries in wavy channels.

In the presented work, two groups of studies are conducted using channels of the same footprint length and cross-sectional dimensions. The first group (study 1) focuses on wavy channels with four wavelengths of 850, 1000, 1500, 2000, and 2500 μm and a constant amplitude of 500 μm. In the second group (study 2), the channels have a fixed wavelength of 1000 μm and four amplitudes of 200, 250, 333, and 588 μm. The choice of these values allows the two studies to share the same wave aspect ratio (γ) of 0.2, 0.25, 0.33, 0.5, and 0.588. These configurations are tested with 10 vol.% NPC slurries and inlet velocities of 0.32 m/s and 0.42 m/s. For each combination of the wave aspect ratio and inlet velocity, simulations are carried out under a number of heat fluxes ranging from 1.0×10^4 W/m^2 to 3.0×10^4 W/m^2. The optimal heat flux, identified when the peak Nu_{ratio} occurs, is plotted in Figure 10a. The corresponding maximum Nusselt number, pressure drop, and *TPF* are plotted in Figure 10b, Figure 10c, and Figure 10d, respectively, as a function of the wave aspect ratio.

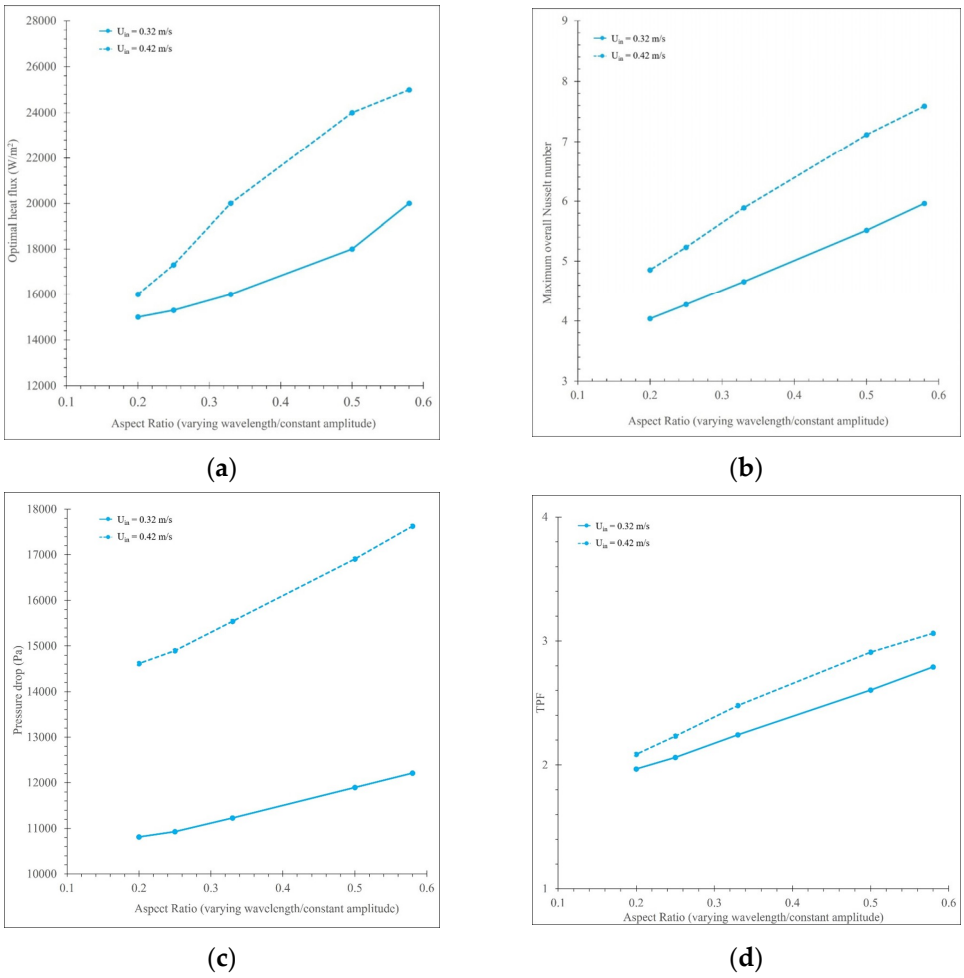

Figure 10. Variations in (**a**) optimal heat flux; (**b**) maximum overall Nusselt number; (**c**) pressure drop; and (**d**) *TPF* with aspect ratios of varying wavelength in study group 1.

In study 1, when the wavelength decreases from 2500 to 850 μm, the aspect ratio increases from 0.2 to 0.588, and the maximum curvature increases from 1/633 to 1/73 μm, as listed in Table 4. This leads to an increase in the *De* number by 190% (from 12.11 to 35.65) and 195% (from 15.89 to 46.79), respectively, for the inlet velocities of 0.32 and 0.42 m/s. As a result, both optimal heat flux and the corresponding Nusselt numbers exhibit a significant increase with the aspect ratios, γ, as plotted in Figures 10a and 10b, respectively. The optimal heat flux increases by 33.3% (from 1.5×10^4 to 2.0×10^4 W/m^2), and the Nusselt number increases by 47.5% (from 4.04 to 5.96) for the inlet velocity of 0.32 m/s. For the higher inlet velocity of 0.42 m/s, the effect of the enlarged wave aspect ratio is even more pronounced, as evidenced by the 56.3% increase (from 1.6×10^4 to 2.5×10^4 W/m^2) in the optimal heat flux and the 54.49% increase (from 4.85 to 7.59) in the Nusselt number.

Figures 10c and 10d show the variations in the pressure drop and the thermal performance factor (*TPF*) with the wave aspect ratio (0.2–0.588), respectively. For the inlet velocities of 0.32 and 0.42 m/s, the respective increase in the pressure drop is 12.93% (from 10,814 Pa to 12,203) and 20.63% (from 14,616 to 17,631 Pa). For these inlet velocities, the respective increase in the *TPF* is 41.62% (from 1.97 to 2.79) and 46.41% (from 2.09 to 3.06). The upward trends of the *TFP* with the increasing wave aspect ratio confirm the overall benefit of wavy channels with high wave aspect ratios.

Table 4. The results of optimal heat flux, overall Nusselt number, pressure drop, and *TPF* for aspect ratios 0.2 and 0.588, with the corresponding radius of curvature, *De* number, and inlet velocity.

Parameters (μm)	γ (A/λ)	R_c (μm)	U_{in} (m/s)	*De*	q'' (Optimal) (W/m^2)	$\overline{Nu}$	Δp (Pa)	*TPF*
Study 1: Varying wavelength/constant amplitude, A = 500 μm								
λ = 2500	0.2	633	0.32	12.11	1.5×10^4	4.04	10,814	1.97
			0.42	15.89	1.6×10^4	4.85	14,616	2.09
λ = 850	0.588	73	0.32	35.65	2.0×10^4	5.96	12,213	2.79
			0.42	46.79	2.5×10^4	7.59	17,631	3.06
Study 2: Varying amplitude/constant wavelength, λ = 1000 μm								
A = 200	0.2	253	0.32	19.15	1.5×10^4	4.35	11,310	2.08
			0.42	25.13	1.6×10^4	5.17	15,704	2.17
A = 588	0.588	86	0.32	32.84	1.9×10^4	5.78	11,924	2.72
			0.42	43.11	2.5×10^4	7.42	16,957	3.03

Study 2 evaluates the effects of the wave aspect ratio γ (0.2–0.588) by varying the amplitude A (200–588 μm) while maintaining a constant wavelength λ (1000 μm). With the increasing aspect ratio (from 0.2 to 0.588), the observed trends in the main parameters, such as the optimal heat flux and the corresponding maximum Nusselt number, pressure drop, and thermal performance factor, are similar to the results of study 1. Therefore, the plots are not presented here. Instead, the results are given in Table 4.

We then compare the effects of varying wave wavelength or amplitude on heat transfer performance at two wave aspect ratios (0.2 and 0.588) for the velocity of 0.32 m/s and 0.42 m/s, as listed in Table 4. When the aspect ratio increases from 0.2 to 0.58, the optimal heat flux also increases, and its value is more affected by the aspect ratio when the inlet velocity is larger. Therefore, the percentage difference in the optimal heat flux, Nusselt number, pressure drop, and *TPF* values with the same aspect ratio are calculated.

For the aspect ratio of 0.2, the optimal heat flux in studies 1 and 2 are the same. However, other parameters in study 2, such as the Nusselt number, pressure drop, and *TPF*, are consistently higher than in study 1. For the inlet velocities of 0.32 m/s and 0.42 m/s, the respective Nusselt numbers in study 2 are 7.67% (4.35 vs. 4.04) and 6.60% (5.17 vs. 4.85) higher than in study 1, and the respective pressure drops in study 2 are 4.59% (11,310 vs. 10,814 Pa) and 7.44% (15,704 vs. 14,616 Pa) higher than in study 1. These trends are expected, considering the difference in the maximum curvature of the wavy channels, which is 1/633 μm in study 1 vs. 1/253 in study 2. The *De* number in study 2 is 58.13% (19.15 vs. 12.11) and 58.15% (25.13 vs. 15.89) higher than in study 1 for the inlet velocities of 0.32 m/s and 0.42 m/s, respectively. Combining the increases in both the Nusselt number and pressure drop, the last column of Table 4 gives the thermal performance factor (*TPF*) value to evaluate whether a corresponding combination of parameters is cost effective. It is calculated that the *TPF* value in study 2 is 5.58% (2.08 vs. 1.97) and 3.83% (2.17 vs. 2.09) higher than in study 1 for an inlet velocity of 0.32 m/s and 0.42 m/s, respectively.

For the wave aspect ratio of γ = 0.588, the optimal heat fluxes are similar to each other for both inlet velocities. However, the Nusselt number, pressure drop, and *TPF* in study 1 are slightly higher than study 2, which is the opposite of the observation for γ = 0.2. For the inlet velocities of 0.32 and 0.42 m/s, the respective Nusselt numbers in study 1 are 3.11% (5.96 vs. 5.78) and 2.29% (7.59 vs. 7.42) higher than in study 2, and the respective pressure drops in study 1 are 2.42% (12,213 vs. 11,924 Pa) and 3.94% (17,631 vs. 16,957 Pa) higher than in study 2. The higher values of these parameters are observed in study 1 because of the larger maximum curvature of 1/73 in study 1 compared with the corresponding value of 1/86 μm in study 2. The *De* numbers in study 1 are 8.56% (35.65 vs. 32.84) and 8.54%

(46.79 vs. 43.11) higher than in study 2 for the inlet velocities of 0.32 m/s and 0.42 m/s, respectively. Finally, the *TPF* values in study 1 are 2.57% (2.79 vs. 2.72) and 0.99% (3.06 vs. 3.03) higher than in study 2 for 0.32 m/s and 0.42 m/s inlet velocity, respectively.

It is worth noting that the percentage differences in the results between study 1 and 2 are insignificant. For the wave aspect ratio of γ = 0.2, the optimal heat fluxes in study 1 and 2 are the same, and less than an 8% difference is observed in the Nusselt numbers, pressure drop, and *TPF* with both inlet velocities. For the higher aspect ratio of γ = 0.588, the percentage differences in these parameters are even smaller, within 5% for both velocities. This insignificant difference suggests that varying the wavelength or the amplitude achieves a similar outcome for each given wave aspect ratio.

One limitation of current study is the assumption of well-dispersed nanoparticles. Realistically, the agglomeration of nanoparticles is hard to prevent due to the strong van de Waals attractive force between particles, even after coating particles with dispersants and applying energetic sonication. However, modeling particle agglomeration is a challenging task due to the large number of nanoparticles, the uncertainty of the size distribution, and the difficulty of measuring surface properties such as zeta potential. Therefore, agglomeration is not considered in this work, much like many other simulations of nano/micro-encapsulated phase change materials in the existing literature [20–22,25,34]. Due to this simplification, we believe that the simulated results show the upper limit of heat transfer enhancement with these phase change materials.

4. Conclusions

One limitation of using nano-encapsulated phase change (NPC) slurries as the working fluid in straight microchannels is that the heat transfer enhancement rate decreases with increasing flow rates. The simulation results presented in this study demonstrate that wavy channels have great potential in heat transfer enhancement at elevated flow rates. The wavy flow path induces Dean vortices on the planes normal to the main stream, intensifies the mixing of the NPC slurries, enlarges the fraction of the melted NPCS, and ultimately enhances the heat transfer efficiency. Most importantly, Dean vortices strengthen at higher mainstream velocities, resulting in better heat transfer enhancement with larger flow rates. Furthermore, the heat transfer enhancement induced by NPC slurries varies with the imposed heat flux and flow rate. Interestingly, the maximum heat transfer enhancement obtained with the wavy channels not only exceeds the straight ones but also occurs at a higher heat flux and/or a faster flow rate. Despite the increased pressure drops, the cost-effectiveness assessment using the thermal performance factor confirms the better performance of the wavy channels than the straight ones with NPCS. This finding demonstrates the advantage of wavy channels in the management of intensive heat fluxes with NPC slurries.

The study of the wavy channel configuration (wave aspect ratio) demonstrates significantly improved heat transfer performance, as evidenced by the increases in the optimal heat fluxes and Nusselt numbers when the wave aspect ratio increases from 0.2 to 0.58. Although a larger aspect ratio requires more pump power to drive the fluid through the channel, the overall *TPF* value still increases. Additionally, the aspect ratio can be adjusted by the wavelength and/or the wave amplitude, but these different approaches only result in a very minor difference in the channel performance, manifested by the values of optimal heat flux, *Nu*, pressure drop, and *TPF*.

Author Contributions: Conceptualization and planning of the work presented in the manuscript were conducted by all contributing authors. R.M. contributed to methodology and M.M.Z. contributed to all CFD simulations. Data analysis was performed by R.M., L.Z. and M.M.Z. R.M. and L.Z. supervised and edited the final draft of the manuscript. All authors have read and agreed to the published version of the manuscript.

Funding: This research received no external funding.

Data Availability Statement: The original contributions presented in the study are included in the article, further inquiries can be directed to the corresponding author.

Conflicts of Interest: The authors declare no conflicts of interest.

References

1. Yeh, L.T. Review of heat transfer technologies in electronic equipment. *J. Electron. Packag.* **1995**, *117*, 333–339. [CrossRef]
2. U.S. Air Force. *U.S. Air Force Avionics Integrity Program Notes*; U.S. Air Force: Washington, DC, USA, 1989.
3. Murshed, S.M.M.; Castro, C.A. A critical review of traditional and emerging techniques and fluids for electronics cooling. *Renew. Sustain. Energy Rev.* **2017**, *78*, 821–833. [CrossRef]
4. Naphona, P.; Wiriyasarta, S.; Wongwisesb, S. Thermal cooling enhancement techniques for electronic components. *Int. Commun. Heat Mass Transf.* **2015**, *61*, 140–145. [CrossRef]
5. Shendel, M.D.; Mahalle, A. Cooling of Electronic Equipments with Heat Sink: A Review of Literature. *J. Mech. Civ. Eng.* **2013**, *5*, 56–61.
6. Tullius, J.F.; Vajtai, R.; Bayazitoglu, Y. A review of cooling in microchannel. *Heat Transf. Eng.* **2011**, *32*, 527–541. [CrossRef]
7. Wei, X.; Joshi, Y.; Patterson, M.K. Experimental and Numerical Study of a Stacked Microchannel Heat Sink for Liquid Cooling of Microelectronic Devices. *J. Heat Transf.* **2007**, *129*, 1432–1444. [CrossRef]
8. Tuckerman, D.B.; Pease, R.F.W. High-performance heat sinking for VLSI. *IEEE Electron Device Lett.* **1981**, *2*, 126–129. [CrossRef]
9. Delgado, M.; Lázaro, A.; Mazo, J.; Marín, J.M.; Zalba, B. Experimental analysis of a microencapsulated PCM slurry as thermal storage system and as heat transfer fluid in laminar flow. *Appl. Therm. Eng.* **2012**, *36*, 370–377. [CrossRef]
10. Chai, L.; Shaukata, R.; Wangd, L.; Wanga, H.S. A review on heat transfer and hydrodynamic characteristics of nano/microencapsulated phase change slurry (N/MPCS) in mini/microchannel heat sinks. *Appl. Therm. Eng.* **2018**, *135*, 334–349. [CrossRef]
11. Lin, Y.; Jia, Y.; Alva, G.; Fang, G. Review on thermal conductivity enhancement, thermal properties and applications of phase change materials in thermal energy storage. *Renew. Sustain. Energy Rev.* **2018**, *82*, 2730–2742. [CrossRef]
12. Roberts, N.S.; Al-Shannaq, R.; Kurdi, J.; Al-Muhtaseb, S.A.; Farid, M.M. Efficacy of using slurry of metal-coated microencapsulated PCM for cooling in a micro-channel heat exchanger. *Appl. Therm. Eng.* **2017**, *122*, 11–18. [CrossRef]
13. Ho, C.J.; Chen, W.C.; Yan, W.M. Correlations of heat transfer effectiveness in a minichannel heat sink with water-based suspensions of Al_2O_3 nanoparticles and/or MEPCM particles. *Int. J. Heat Mass Transf.* **2014**, *69*, 293–299. [CrossRef]
14. Ho, C.J.; Chen, W.C.; Yan, W.M. Experimental study on cooling performance of minichannel heat sink using water-based MEPCM particles. *Int. Commun. Heat Mass Transf.* **2013**, *48*, 67–72. [CrossRef]
15. Dammel, K.; Stephan, P. Heat transfer to suspensions of microencapsulated phase change material flowing through minichannels. *J. Heat Transf.* **2012**, *134*, 020907–020915. [CrossRef]
16. Rao, Y.; Dammel, F.; Stephan, P. Experiments on cooling performance of microencapsulated phase change material suspension flow in rectangular minichannels. *ASME-JSME Therm. Eng. Summer Heat Transf. Conf.* **2007**, *2*, 569–573.
17. Hasan, M.; Tbena, H.L. Using of phase change materials to enhance the thermal performance of micro channel heat sink. *Eng. Sci. Technol. Int. J.* **2018**, *21*, 517–526. [CrossRef]
18. Liu, C.; Rao, Z.; Zhao, J.; Huo, Y.; Li, Y. Review on nano encapsulated phase change materials: Preparation, characterization, and heat transfer enhancement. *Nano Energy* **2015**, *13*, 814–826. [CrossRef]
19. Sabbaghi, S.; Mehravar, S. Effect of using nano encapsulated phase change material on thermal performance of micro heat sink. *Int. J. Nanosci. Nanotechnol.* **2015**, *11*, 33–38.
20. Seyf, H.R.; Zhou, Z.; Ma, H.B.; Zhang, Y. Three-dimensional numerical study of heat-transfer enhancement by nano-encapsulated phase change material slurry in microtube heat sinks with tangential impingement. *Int. J. Heat Mass Transf.* **2013**, *56*, 561–573. [CrossRef]
21. Alquaity, A.; Al-Dini, S.A.; Wang, E.; Yilbas, B.S. Numerical investigation of liquid flow with phase change nanoparticles in microchannels. *Int. J. Heat Fluid Flow* **2012**, *38*, 159–167. [CrossRef]
22. Sabbah, R.; Seyed-Yagoobi, J.; Al-Hallaj, S. Heat transfer characteristics of liquid flow with micro-encapsulated phase change material: Numerical study. *J. Heat Transf.* **2011**, *133*, 121702–121712. [CrossRef]
23. Xing, K.Q.; Hao, Y.L.; Tao, Y.X. Performance evaluation of liquid flow with PCM particles in microchannels. *J. Heat Transf.* **2005**, *127*, 931–940. [CrossRef]
24. Hao, Y.L.; Tao, Y.X. A numerical model for phase change suspension flow in microchannels. *Numer. Heat Transf. Appl.* **2004**, *46*, 55–77. [CrossRef]
25. Kuravi, S.; Kota, K.M.; Du, J.; Chow, L. Numerical investigation of flow and heat transfer performance of nano-encapsulated phase change material slurry in microchannels. *J. Heat Transf.* **2009**, *131*, 0629011–0629019. [CrossRef]
26. Mohit, M.K.; Gupta, R. Numerical investigation of the performance of rectangular micro-channel equipped with micro-pin-fin. *Case Stud. Therm. Eng.* **2022**, *32*, 101884. [CrossRef]
27. Xue, Y.; Ge, Z.; Du, X.; Yang, L. On the heat transfer enhancement of plate fin heat exchanger. *Energies* **2018**, *11*, 1398. [CrossRef]
28. Chai, L.; Xia, G.; Wang, L.; Zhou, M.Z.; Cui, Z. Heat transfer enhancement in microchannel heat sinks with periodic expansion–constriction cross-sections. *Int. J. Heat Mass Transf.* **2013**, *62*, 741–751. [CrossRef]

29. Ho, C.J.; Hsu, S.; Rashidi, S.; Yan, W.M. Water-based nano-PCM emulsion flow and heat transfer in divergent mini-channel heat sink—An experimental investigation. *Int. J. Heat Mass Transf.* **2020**, *148*, 119086. [CrossRef]
30. Qiu, Z.; Li, L. Experimental and numerical investigation of laminar heat transfer of microencapsulated phase change material slurry (MPCMS) in a circular tube with constant heat flux. *Sustain. Cities Soc.* **2020**, *52*, 101786. [CrossRef]
31. Liu, Y.; Li, Q.; Nie, D. Two-dimensional numerical study on the migration of particle in a serpentine channel. *J. Nanotechnol.* **2018**, *8*, 2615404. [CrossRef]
32. Sui, Y.; Teo, C.J.; Lee, P.S.; Chew, Y.T.; Shu, C. Fluid flow and heat transfer in wavy microchannels. *Int. J. Heat Mass Transf.* **2010**, *53*, 2760–2772. [CrossRef]
33. Santhosh Reddy, V.; Venkatachalapathy, S.; Nanda Kishore, P.V.R. Study on thermal performance and flow behavior of myristyl alcohol phase change material microencapsulated with hybrid shell in minichannels. *Appl. Therm. Eng.* **2024**, *124138*, 1359–4311. [CrossRef]
34. Sabbah, R.; Farid, M.M.; Al-Hallaj, S. Micro-channel heat sink with slurry of water with micro-encapsulated phase change material: 3D-numerical study. *Appl. Therm. Eng.* **2009**, *29*, 445–454. [CrossRef]
35. Morini, G.; Spiga, M. The role of the viscous dissipation in heated microchannels. *J. Heat Transf.* **2007**, *129*, 308–318. [CrossRef]
36. Webb, R.L. Performance evaluation criteria for use of enhanced heat transfer surfaces in heat exchanger design. *Int. J. Heat Mass Transf.* **1981**, *24*, 715–726. [CrossRef]
37. Saha, S.K.; Tiwari, M.; Sundén, B.; Wu, Z. *Advances in Heat Transfer Enhancement*; Springer: Cham, Switzerland, 2016.
38. Kumar, S.R.; Singh, S. Numerical analysis for augmentation of thermal performance of single-phase flow in microchannel heat sink of different sizes with or without micro-inserts. *Fluids* **2022**, *7*, 149. [CrossRef]
39. Alisetti, E.L.; Roy, S.K. Forced convection heat transfer to phase change material slurries in circular ducts. *J. Thermophys. Heat Transf.* **2022**, *14*, 115–118. [CrossRef]
40. Vand, V. Theory of viscosity of concentrated suspensions. *Nature* **1945**, *155*, 364–365. [CrossRef]
41. Maxwell, J.C. *A Treatise on Electricity and Magnetism*, 3rd ed.; Dover: New York, NY, USA, 1954; Volume 1, pp. 440–441.
42. Buongiorno, J.; Venerus, D.; Prabhat, N.; McKrell, T.; Townsend, J.; Christianson, R.; Tolmachev, Y.; Keblinski, P.; Wen, D.; Alvarado, J.; et al. A benchmark study on the thermal conductivity of nanofluids. *J. Appl. Phys.* **2009**, *106*, 094312. [CrossRef]
43. Rajabifar, B. Enhancement of the performance of a double layered microchannel heatsink using PCM slurry and nanofluid coolants. *Int. J. Heat Mass Transf.* **2015**, *88*, 627–635. [CrossRef]
44. Rajabifar, B.; Seyf, R.H.; Zhang, Y.; Khanna, S.K. Flow and heat transfer in micro pin fin heat sinks with nano-encapsulated phase change materials. *J. Heat Transf.* **2016**, *138*, 062401. [CrossRef]
45. Sui, Y.; Lee, P.S.; Teo, C.J. An experimental study of flow friction and heat transfer in wavy microchannels with rectangular cross section. *Int. J. Therm. Sci.* **2011**, *50*, 2473–2482. [CrossRef]
46. Wang, Y.; Chen, Z.; Ling, X. An experimental study of the latent functionally thermal fluid with micro-encapsulated phase change material particles flowing in microchannels. *Appl. Therm. Eng.* **2016**, *105*, 209–216. [CrossRef]
47. Incropera, F.; DeWitt, D. *Fundamentals of Heat and Mass Transfer*, 6th ed.; J. Wiley & Sons: New York, NY, USA, 2007.
48. Zhu, J.F.; Li, X.Y.; Wang, S.L.; Yang, Y.R.; Wang, X.D. Performance comparison of wavy microchannel heat sinks with wavy bottom rib and side rib designs. *Int. J. Therm. Sci.* **2019**, *146*, 106068. [CrossRef]
49. Sahar, A.M.; Wissink, J.; Mahmoud, M.M.; Karayiannis, T.G.; Ishak, M.A. Effect of hydraulic diameter and aspect ratio on single phase flow and heat transfer in a rectangular microchannel. *Appl. Therm. Eng.* **2017**, *115*, 793–814. [CrossRef]
50. Lin, L.; Zhao, j.; Lu, g.; Wang, X.D.; Yan, W.M. Heat transfer enhancement in microchannel heat sink by wavy channel with changing wavelength/amplitude. *Int. J. Therm. Sci.* **2017**, *118*, 423–434. [CrossRef]
51. Zhou, J.; Hatami, M.; Song, D.; Jing, D. Design of microchannel heat sink with wavy channel and its time-efficient optimization with combined RSM and FVM methods. *Int. J. Heat Mass Transf.* **2016**, *103*, 715–724. [CrossRef]
52. Xie, G.N.; Chen, Z.Y.; Sunden, B.; Zhang, W.H. Comparative study of the flow and thermal performance of liquid-cooling parallel-flow and counter-flow double-layer wavy microchannel heat sinks. *Int. J. Comput. Methodol.* **2013**, *64*, 30–55. [CrossRef]
53. Mohammed, H.A.; Gunnasegaran, P.; Shuaib, N.H. Numerical simulation of heat transfer enhancement in wavy microchannel heat sink. *Int. Commun. Heat Mass Transf.* **2011**, *38*, 63–68. [CrossRef]
54. Ghorbani, N.; Targhi, M.Z.; Heyhat, M.M.; Alihosseini, Y. Investigation of wavy microchannel ability on electronic devices cooling with the case study of choosing the most efficient microchannel pattern. *Sci. Rep.* **2022**, *12*, 5882. [CrossRef]

Disclaimer/Publisher's Note: The statements, opinions and data contained in all publications are solely those of the individual author(s) and contributor(s) and not of MDPI and/or the editor(s). MDPI and/or the editor(s) disclaim responsibility for any injury to people or property resulting from any ideas, methods, instructions or products referred to in the content.